Journal of Alloys and Compounds 509 (2011) 5211–5215

Contents lists available at ScienceDirect

Journal of Alloys and Compounds

journal homepage: www.elsevier.com/locate/jallcom

Fabrication and thermoelectric properties of crystal-aligned nano-structured Bi_2Te_3

Dong-Hwan Kim [a], Cham Kim [a], Dong-Woo Ha [b], Hoyoung Kim [a,*]

[a] Daegu Gyeongbuk Institute of Science and Technology (DGIST), 223 Sang-Ri, Hyeonpung-Myeon, Dalseong-gun, Daegu 704-948, Republic of Korea
[b] Korea Electrotechnology Research Institute (KERI), 28-1 Sengju-dong, Changwon-si, Gyeongsangnam-do, 641-120, Republic of Korea

ARTICLE INFO

Article history:
Received 4 January 2011
Received in revised form 10 February 2011
Accepted 10 February 2011
Available online 17 February 2011

Keywords:
Thermoelectric
Nanostructure
Crystal alignment
High magnetic field
Spark plasma sintering

ABSTRACT

With a view to experimental demonstration for an improved thermoelectric performance, a slip casting method under high magnetic field for uni-directionally aligned crystals has been investigated. The sintered body of Bi_2Te_3 powder, its size between 300 and 500 nm, green-bodied under 6 T magnetic field showed a 33% variation in the fraction of the directionally aligned crystals. According to increasing this fraction, electrical resistivity was reduced with keeping thermal conductivity and Seebeck coefficient unchanged. This could be explained from the fact that the aligned crystals by magnetic field has increased the carrier mobility keeping carrier concentration unchanged.

1. Introduction

Thermoelectric materials are known as materials at which electricity is generated directly from heat and vice versa without combining any moving elements or any environmentally harmful fluid. Owing to simplicity in device, silence at operation, and high reliability thermoelectric technology has been utilized for space power generation and precise temperature control applications. However, low efficiency in energy conversion has prevented wider usage of this thermoelectric technology. The comprehensive performance of thermoelectric materials is evaluated in terms of non-dimensional figure-of-merit ZT, which is a function of the electrical resistivity (ρ), Seebeck coefficient (α) and thermal conductivity (κ) in the following relationship: $ZT = (\alpha^2/\rho k)T$ [1].

Nanotechnology has opened possibility to improve thermoelectric performance of materials with the knowledge of quantum dots [2], superlattices [3,4], nanowires [5], and nanocomposites [6,7]. The role of the well-organized nanostructures in thermoelectric materials has been understood in that they restrict phonon motions and thus lower thermal conductivity [8].

In polymeric and ceramic materials of paramagnetism and/or diamagnetism with magnetic anisotropy, highly textured microstructures have been fabricated by colloidal processing under strong magnetic field followed by appropriate heat and/or mechanical treatments. The textured microstructure improved physical and mechanical properties [9,10]. Several thermoelectric materials like $MnSi_{2-x}$ [11], aluminum doped ZnO [12], calcium–cobalt oxide [13] and *n*-type Bi_2Te_3 [14] have been investigated with the above magnetic texturing method. Their results showed a possibility to reduce the electric resistivity owing to the uni-directionally aligned crystals.

Many studies have been reported for thermoelectric materials of textured crystals processed via hot forging, template grain growth, hot extrusion and so forth [15–19]. These processes utilized force and/or temperature gradient at high temperature at which grain growth accompanied with recrystallization and/or diffusion was inevitable.

Bi–Te compounds possess a layered hexagonal structure comprised of five atom stacks of Te–Bi–Te–Bi–Te, and the Te–Te layers are bonded by a weak van der Waals force. It is well known that these materials have thermoelectric anisotropy originated from this structural anisotropy [20]. Delves and co-workers first reported on the anisotropy of the electrical resistivity with single crystal Bi_2Te_3 between along van der Waals boding plane and along the direction perpendicular to the bonding plane [21]. Their experimental measurements indicated that the electrical resistivity along the van der Waals bonding plane was smaller than that along the direction perpendicular to the bonding plane. They obtained approximately a factor of 3.2 for the ratio of ρ_{33}/ρ_{11}, where subscript 11 denotes the value measured along the van der Waals bonding plane and 33 measured along the direction perpendicular to the bonding plane. The thermal conductivity is understood

* Corresponding author. Tel.: +82 54 770 2936; fax: +82 54 770 2940.
E-mail addresses: hoykim@dgist.ac.kr, kimdhwan@dgist.ac.kr (H. Kim).

0925-8388/$ – see front matter © 2011 Elsevier B.V. All rights reserved.
doi:10.1016/j.jallcom.2011.02.059

that it can be decomposed into a lattice vibration contribution and a free electronic contribution, where this electronic contribution is directly related to the carrier concentration and mobility. In case of Seebeck coefficient, it is known as reasonably isotropic and dependent on the carrier concentration. These observations on thermoelectric property of single crystalline Bi–Te system reveal a possibility that thermoelectric performance can be improved by adjusting the crystal orientation of grains in poly crystalline Bi–Te materials.

Based on the above literature survey, we propose a hypothesis to improve thermoelectric performance such that nanostructures with uni-directionally aligned crystals may enjoy both lowering thermal conductivity coming from nanostructure and lowering electric resistivity from crystal alignment. In other words, Wiedemann–Franz relationship can be overcome to improve thermoelectric performance. With a view to experimental demonstration for the hypothesis, wet-chemistry for nano-sized Bi_2Te_3 powder and slip casting method under high magnetic field for uni-directionally aligned crystals has been investigated. The spark plasma sinter machine was employed for sintering the green body since it minimizes the grain growth as much as possible during sintering process [22,23].

2. Experimental details

2.1. Sample preparation

Green bodies of uni-directionally aligned Bi_2Te_3 were fabricated through slip casting with gypsum mold. The Bi_2Te_3 powder, its size between 300 and 500 nm obtained via wet chemistry route, was dispersed in anhydrous ethanol using a high energy ultrasonic probe (Sonics Co. VCX-750) to prepare the dispersed slurry with a solid loading of 35 vol%. Then, the slurry was poured in a cylindrical container and the container was placed horizontal in the magnetic field of a superconducting magnet (JMT, JMTD-6T100M). The container was made of PET for the side wall and of gypsum for the bottom to absorb out the anhydrous ethanol along the gravitational direction. The container was rotated at 10 rpm under a horizontal magnetic field of 6 T, where the rotating axis was in the gravitational direction. The green bodies with and without the magnetic field were sintered into the cylindrical shape of ϕ15 mm × 12 mm with the spark plasma sintering machine (DR. Sinter, SPS-3 20MK-IV) at 50 MPa, 350 °C for 2 min in Argon atmosphere. The pressing direction coincided to the gravitational direction.

2.2. Characterization

Powder X-ray diffraction (XRD) patterns were collected with a D/MAX-2500 diffractometer (Rigaku) using Cu Kα radiation and a scintillation counter detector. Relevant patterns were recorded over a 2θ range of 20–80°. Field emission scanning electron micrographs (FE-SEM) were obtained using an S-4800 microscope (Hitachi) to observe the powder morphology. Electron backscatter diffraction (EBSD) analysis for the sintered bodies was conducted with a Hitachi S-4300SE scanning electron microscope. The scan area of 20 μm × 20 μm with a step size of 0.03 μm was used at an accelerating voltage of 25 kV. The EBSD samples were prepared with mechanical and vibrational polishing in an aqueous solution containing the colloidal silica particles.

The thermoelectric properties of the sintered bodies were measured in both directions of parallel and perpendicular to the pressing direction. The Hall coefficient, R_H, of 5 mm × 5 mm × 0.3 mm specimens was measured with van der Pauw method at room temperature using Hall measurement system (Ecopia, HMS-3000). Electrical resistivity and Seebeck coefficient of 2 mm × 2 mm × 10 mm specimens were measured simultaneously in the temperature range between 25 and 300 °C using a commercial instrument (Ulvac-Rico ZEM3). Thermal conductivity was evaluated using the relation $\kappa = \lambda \times C_p \times d$, where λ, C_p, and d are thermal diffusivity, specific heat and density, respectively. The thermal diffusivity λ was measured between 25 °C and 300 °C using a laser flash method (Netzsch LFA447). The specific heat and the density were adopted from the values of Bi_2Te_3 [24].

3. Results and discussion

Fig. 1 shows XRD and micrographs of the Bi_2Te_3 powder. According to XRD result, the crystalline pattern exhibited diffraction lines of (006), (101), (015), (1010), (0111), (110), (0015), (205), (208/1016), (0210), (1115), (125), (2110/1022), and (300/0024) planes at 2θ values of 17.2°, 23.4°, 27.5°, 37.7°, 40.6°, 41.0°, 44.6°, 50.2°, 53.7°, 56.9°, 62.1°, 66.9°, 72.7°, and 75.0°, respectively, which precisely coincide with values of the rhombohedral Bi_2Te_3 (JCPDS Card No. 85-0439, 82-0358). The Bi_2Te_3 powder was seen to have nano-size in between 300 and 500 nm (Fig. 1b).

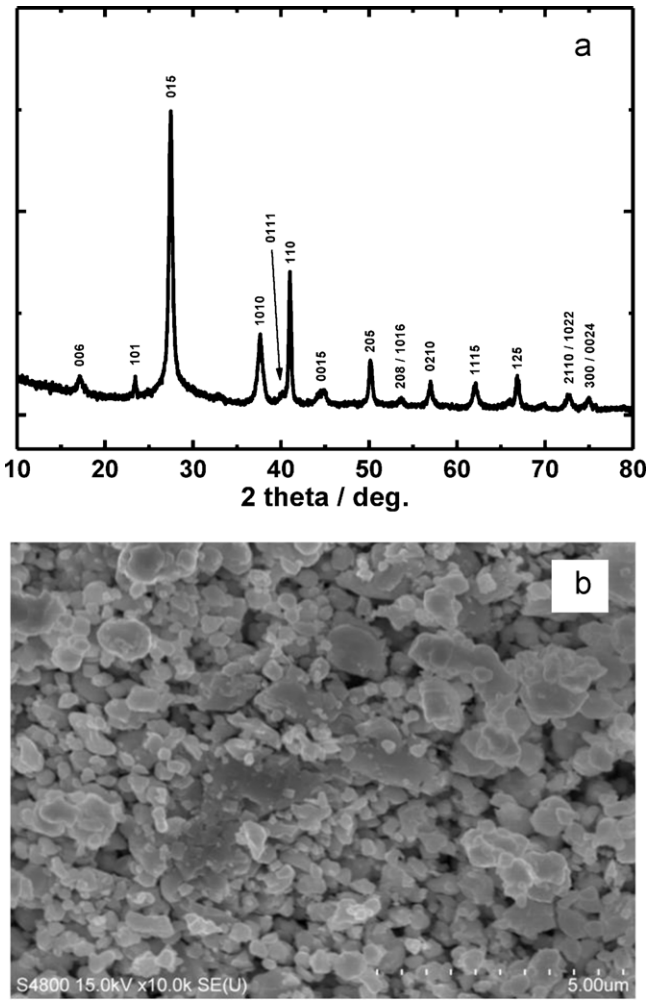

Fig. 1. (a) X-ray diffraction (XRD) patterns and (b) SEM photograph of Bi_2Te_3 powders.

Fig. 2 shows the EBSD mapping images of the sintered bodies. (a) and (b) are for the sintered body without crystal alignment, whereas (c) and (d) for the crystal alignment with magnetic field. (a) and (c) are seen along the pressing direction and (b) and (d) seen perpendicular to of the pressing direction. In the images, the red color was set to the crystal orientation of [0 0 l] planes and the closed areas denote grains. The grain size of both specimens was same in between 400 and 500 nm, no difference originated to the magnetic field treatment. The fractions of aligned crystals to [0 0 l] plane were measured as (a) 12.7%, (b) 1.4%, (c) 16.9%, and (d) 1.0%. The 6 T magnetic field played a role in aligning crystals to [0 0 l] plane and changed the fraction by about 33%; increase at the top surface and decrease at the side surface. Additionally from the results of (a) and (b), it seemed that the dispersion itself contributed to the crystal alignment of Bi_2Te_3 powder.

Figs. 3–5 are electric resistivity, Seebeck coefficient, and thermal conductivity of the sintered bodies, and Table 1 shows the variation of thermoelectric properties in the parallel direction to the SPS pressing direction, where 33 and 11 denote the measured directions parallel and perpendicular to the pressing direction, respectively and 6T and 0T denote slip casting with and without 6 T magnetic field. The electric resistivity in Fig. 3 and Table 1 shows

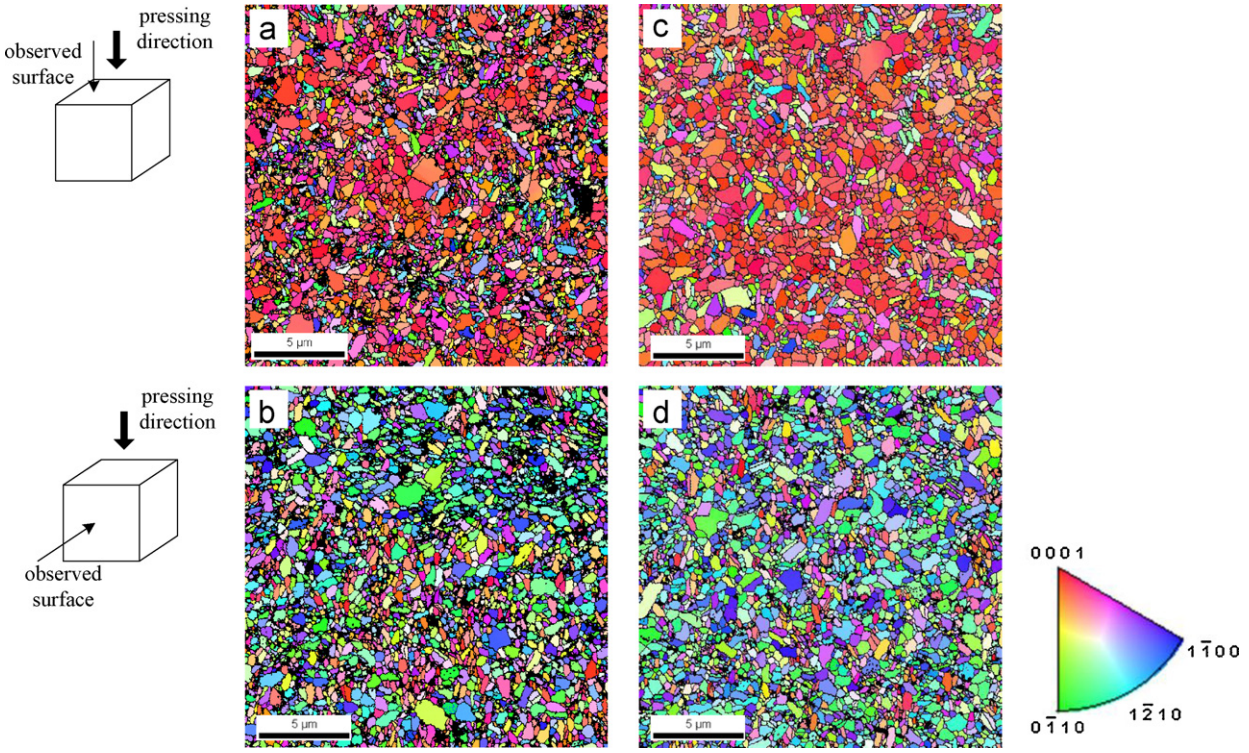

Fig. 2. EBSD mapping images in the area of 20 μm × 20 μm with a step of 0.03 μm: (a) the top and (b) the side surfaces for the sintered body without magnetic field, and (c) the top and (d) the side surface with the magnetic field of 6 T.

Table 1
Variation of thermoelectric properties in the parallel direction to the SPS pressing direction owing to crystal alignment with magnetic field of the sintered body of Bi_2Te_3. 0T and 6T denote the value without/with the magnetic alignment.

Temperature	Electrical resistivity $\frac{\rho_{6T}-\rho_{0T}}{\rho_{0T}}$	Seebeck coefficient $\frac{\alpha_{6T}-\alpha_{0T}}{\alpha_{0T}}$	Thermal conductivity $\frac{\kappa_{6T}-\kappa_{0T}}{\kappa_{0T}}$	ZT $\frac{ZT_{6T}-ZT_{0T}}{ZT_{0T}}$
25	−0.12	−0.01	−0.02	0.14
50	−0.11	−0.02	−0.01	0.10
100	−0.10	−0.01	−0.01	0.10
150	−0.09	0.00	0.01	0.09
200	−0.09	0.00	0.02	0.07
250	−0.08	0.00	0.01	0.08
300	−0.07	0.01	0.01	0.08

that crystal alignment lessened the electric resistivity by 10% in both 11 and 33 directions. Seebeck coefficient shown in Fig. 4 and Table 1 did not show remarkable effects of the crystal alignment, and the same for thermal conductivity in Fig. 5. The differences between 11 and 33 directions seemed the effect of anisotropy in the microstructure shown in Fig. 3.

Non-dimensional figure-of-merit in Fig. 6 and Table 1 shows the enhancement even by 14% owing to the crystal alignment. These observations suggested that the crystal alignment of nano-sized grains made the electric resistivity decreased keeping Seebeck coefficient and thermal conductivity unchanged, and thus figure-of-merit enhanced.

Table 2 gives thermoelectric properties, carrier concentration, and carrier mobility at room temperature without (0T)/with (6T) magnetic alignment of the sintered body of Bi_2Te_3. First of all we can easily find that the so-called Wiedemann–Franz law does not hold any more in crystal alignment of nano-sized grains, that is, electric resistivity has varied considerably with keeping thermal conductivity unchanged. The carrier concentration and Seebeck coefficient showed no remarkable effect of the magnetic field (between 0T and 6T) but showed a slight anisotropy between 11 and 33 directions. However, the carrier mobility showed a considerable effect of the magnetic alignment; the mobility in 11 direction increased by 17% owing to the crystal alignment. These observations qualitatively reflect the relationship between electrical resistivity and

Table 2
Thermoelectric properties at room temperature without (0T)/with (6T) magnetic alignment of the sintered body of Bi_2Te_3. 33 and 11 denote the measured directions parallel and perpendicular to the SPS pressing direction, respectively.

Sample	Carrier concentration (10^{19} cm^{-3})	Electric resistivity (μΩ m)	Seebeck coefficient (μV K^{-1})	Thermal conductivity (W m^{-1} K^{-1})	ZT	Mobility (cm^2 V^{-1} s^{-1})
BTn_0T_11	5.03	7.9	−104	1.03	0.40	157
BTn_0T_33	5.23	9.2	−112	0.95	0.43	130
BTn_6T_11	4.91	6.9	−104	1.01	0.46	184
BTn_6T_33	5.37	8.7	−117	0.94	0.50	134

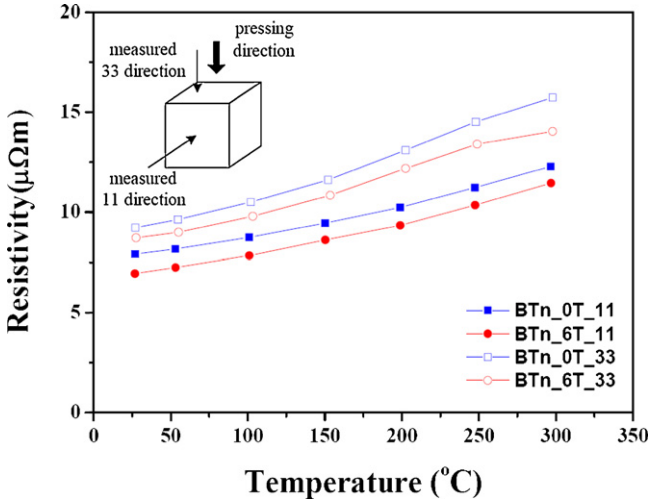

Fig. 3. The electrical resistivity versus temperature of the sintered bodies with (6T) and without (0T) the magnetic field. 33 and 11 denote the measured directions parallel and perpendicular to the SPS pressing direction, respectively.

hole mobility given in Eq. (1) and the expression of Seebeck coefficient known to be dependent on carrier concentration and be independent on mobility given in Eq. (2)

$$\rho \sim \frac{1}{n\mu_H} \tag{1}$$

$$\alpha = \pm\frac{kg}{e}\left((r+2) + \ln\frac{2(2\pi^* k_B T)^{3/2}}{h^{3n}}\right) \tag{2}$$

where, ρ is electric resistivity, n carrier concentration, μ_H carrier mobility, α Seebeck coefficient, k_B Boltzmann's constant, r the scattering factor, m^* effective mass, and h the Plank constant. Comparing to the properties of single crystalline n type Bi_2Te_3 [25], it was easily found that thermal conductivity was relatively low and less anisotropic and that electric resistivity was less anisotropic. Low thermal conductivity was attributed to the phonon scattering at the boundaries of nano-sized grains and less anisotropy was due to the effect of assembly of grains.

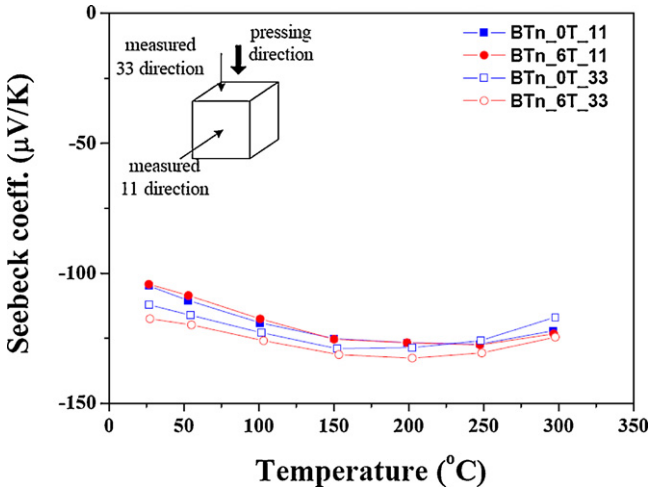

Fig. 4. Seebeck coefficient versus temperature of the sintered bodies with (6T) and without (0T) the magnetic field. 33 and 11 denote the measured directions parallel and perpendicular to the SPS pressing direction, respectively.

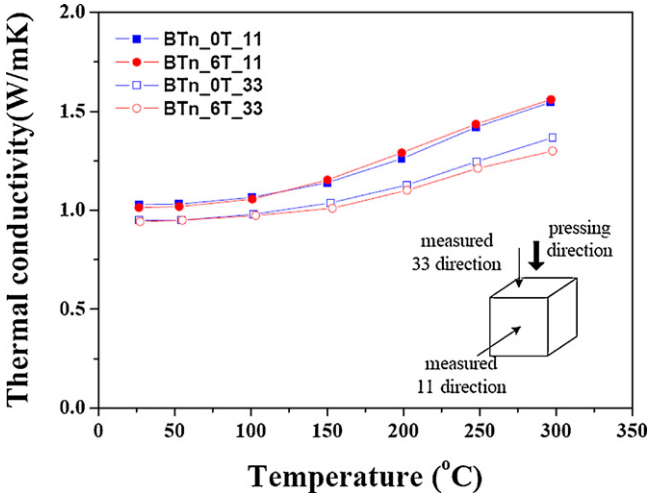

Fig. 5. The thermal conductivity versus temperature of the sintered bodies with (6T) and without (0T) the magnetic field. 33 and 11 denote the measured directions parallel and perpendicular to the SPS pressing direction, respectively.

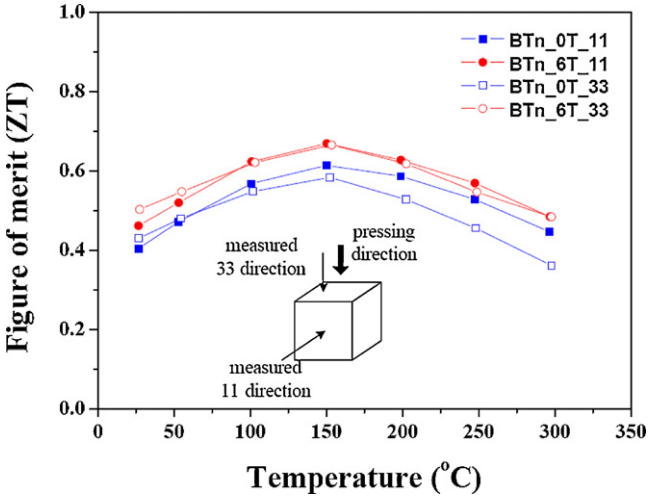

Fig. 6. The figure-of-merit coefficient versus temperature of the sintered bodies with (6T) and without (0T) the magnetic field. 33 and 11 denote the measured directions parallel and perpendicular to the SPS pressing direction, respectively.

4. Conclusions

The sintered body of Bi_2Te_3 nano-sized powder with the 6T magnetic field showed 33% variation in fraction of the directionally aligned crystals. The electric resistivity was reduced with keeping thermal conductivity and Seebeck coefficient unchanged by increasing the fraction of uni-directionally aligned crystals. This could be explained from the fact that crystal alignment induced by magnetic field has improved the carrier mobility keeping carrier concentration unchanged. Based on this experimental work, we concluded that thermoelectric performance of nano-composite Bi_2Te_3 can be improved by aligning crystal orientation with magnetic field.

Acknowledgements

This work was supported by the Energy Efficiency & Resources of the Korea Institute of Energy Technology Evaluation and Planning (KETEP) grant funded by the Ministry of Knowledge Economy, Republic of Korea (No. 2007EID11P050000).

References

[1] A.F. Ioffe, Semiconductor Thermoelements and Thermoelectric Cooling, Infosearch Ltd, London, 1957.
[2] T.C. Harman, P.J. Taylor, D.L. Spears, M.P. Walsh, J. Electron. Mater. 29 (2000) L1.
[3] L.D. Hicks, M.S. Dresselhaus, Phys. Rev. B 47 (1993) 16631.
[4] R. Venkatasubramanian, E. Siivola, T. Colpitts, B. O'Quinn, Nature 413 (2001) 597.
[5] X. Sun, Z. Zhang, M.S. Dresselhaus, Appl. Phys. Lett. 74 (1999) 4005.
[6] B. Poudel, Q. Hao, Y. Ma, Y. Lan, A. Minnich, B. Yu, Z. Yan, D. Wang, A. Muto, D. Vashaee, Z. Chen, J. Liu, M.S. Dresselhaus, G. Chen, Z. Ren, Science 320 (2008) 634.
[7] D.H. Kim, T. Mitani, J. Alloys Compd. 399 (2005) 14.
[8] H.J. Goldsmid, A.W. Penn, Phys. Lett. 27A (1968) 523.
[9] T. Kimura, Polym. J. 35 (2003) 823.
[10] Y. Sakka, T.S. Suzuki, J. Ceram. Soc. Jpn. 113 (2005) 26.
[11] H. Kaga, et al., J. Mater. Res. 22 (2007) 2917.
[12] H. Kaga, et al., J. Ceram. Soc. Jpn. 114 (2006) 1085.
[13] S. Horii, et al., Proc. MRS 2002 Fall DD11 (2002) 30.
[14] T Kuribayashi, M.G. Sung, T. Itoh, K. Sassa, S. Asai, Mater. Trans. 47 (2006) 2387.
[15] T.S. Oh, D.B. Hyun, N.V. Kolomoets, Scr. Mater. 42 (2000) 849.
[16] S.J. Hong, B.S. Chun, Mater. Res. Bull. 38 (2003) 599.
[17] P. Pierrat, A. Dauscher, B. Lenoir, R.M. Lopez, H. Scherrer, J. Mater. Sci. 32 (1997) 3563.
[18] S. Miura, Y. Sato, K. Fukuda, K. Nishimura, K. Ikeda, Mater. Sci. Eng. A277 (2000) 244.
[19] J. Seo, K. Park, D. Lee, C. Lee, Mater. Sci. Eng. B49 (1997) 247.
[20] J.R. Wiese, L. Muldawer, J. Phys. Chem. Solids 15 (1960) 13.
[21] R.T. Delves, A.E. Bowley, D.W. Hazelden, H.J. Goldsmid, Proc. Phys. Soc. 78 (1961) 838.
[22] L. Yucheng, A.J. Minnich, G. Chen, Z. Ren, Adv. Funct. Mater. 20 (2010) 357.
[23] M. Scheele, N. Oeschler, K. Meier, A. Kornowski, C. Klinke, H. Weller, Adv. Funct. Mater. 19 (2009) 3476.
[24] M. Binnewies, E. Milke, Thermochemical Data of Elements and Compounds, vol. 168, Wiley-VCH, 2002, p. 829.
[25] J.P. Fleurial, L. Gailliard, R. Triboulet, H. Scherrer, S. Scherrer, J. Phys. Chem. Solids 49 (1988) 1237.